# Ionospheric Correlation Analysis for WAAS: Quiet and Stormy

Andrew Hansen Juan Blanch Todd Walter Per Enge

*Stanford University*

## ABSTRACT

Dual-frequency measurements made with wide area GPS reference networks provide extremely precise and geographically diverse observations of the ionosphere. While these measurements amount to integrals along a line of sight, coordinated measurements can be brought into a single observation framework for modelling the ionosphere. In WAAS, one this is accomplished with one simplifying assumption, namely the thin-shell approximation. While this approximation has some limitations it is suitable for many applications, one of which is the ionospheric differential correction in the Federal Aviation Administration's Wide Area Augmentation System (WAAS) for GPS. The WAAS application was in fact the motivation for this correlation analysis. The correlation model directly supports the ionospheric irregularity detection process as part of the WAAS integrity algorithms. Beyond WAAS, we feel that both the procedures and the results would be useful to the general ionospheric community who have a great deal of GPS data readily available or would like to fuse disparate data sources together.

We give here a description of the measurement processing for noise and multipath removal via a triple threaded reference network, the extended additive model, and its utility in the irregularity detector. We present correlation analyses of measurements made during both nominal (quiet) and disturbed (stormy) ionospheric conditions. In particular, we address the ionospheric activity that occurred 6-8 April 2000 and 15-16 July 2000. This data represents the most extreme conditions yet experienced in the current solar cycle.

## INTRODUCTION

The ionospheric correction process in the Wide Area Differential GPS (WADGPS) concept for aviation relies upon the construction of a real-time model of the ionospheric effect on GPS signals. This model necessarily covers a large geographic scale for the system to be viable because the same corrections are broadcast to users across continental separations. This process has been well outlined in the literature [1], in particular for aviation [2]. An underlying tenet of the aviation application is protection of the residual error in the correction process. Indeed the vast majority of the development effort for the FAA's Wide Area Augmentation System (WAAS) is devoted to designing algorithms that generate, again in real-time, protection limits for the residual position error in the differential correction to GPS [3].

Development of the WAAS is motivated by the safety and economic benefits to navigation users afforded by having four-dimensional position information available on demand. This end user base includes not only aviation users but any mobile user in need of real-time navigation. An integral part of the WAAS is the ionospheric correction which improves the fundamental accuracy of the system and is explicitly necessary for precision approach where the WAAS is providing vertical guidance to the aircraft. In this situation the requirement on the differential correction error bound, or vertical protection limit (VPL), is very stringent. As written, the probability that the WAAS vertical position error exceeds the VPL shall be less than $10^{-7}$ per approach. Practically, if the VPL fails to cover the the vertical error, the system is said to have lost integrity.

The correlation concepts presented below support both the estimation and integrity algorithms in WAAS ionospheric correction and can be split across two dimensions, order and condition. In the former we have identified correlation expressions for a $0^{th}$ order and a $1^{st}$ order ionospheric model which aid both ionospheric estimation and detection of disturbed conditions respectively. In the latter we draw clear distinctions between nominal and

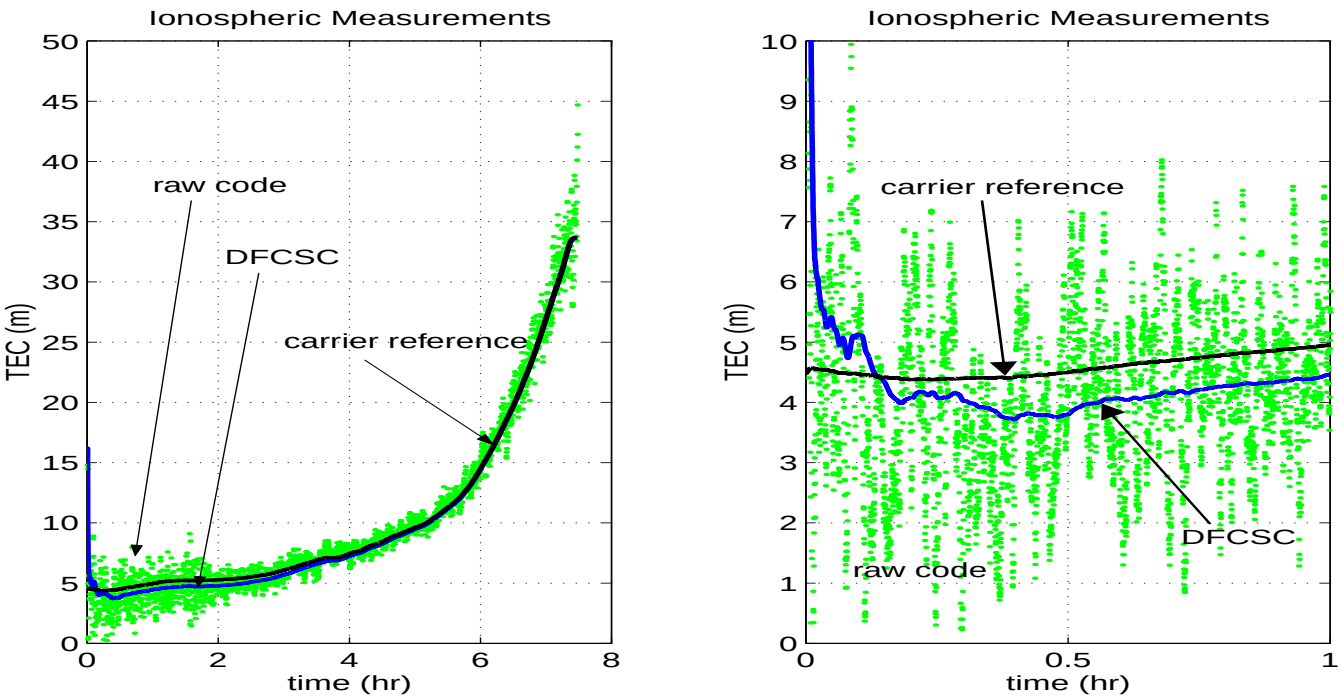


Figure 1: The graph on the left contains the time history of the TEC for a complete satellite pass for three GPS measurements from a single GPS dual frequency receiver: raw pseudorange difference, $\text{TEC}_\rho$, real-time carrier smoothing, and post processed carrier reference. The chart on the right is a close-up of the early portion of the satellite pass where the real-time filter is converging.

disturbed ionospheric conditions directly from the reference station measurements. The ionospheric estimation process will utilize the correlation of the raw vertical ionosphere identified in the $0^{th}$ order model. The ionospheric integrity process will utilize the correlation of the planar residual ionosphere identified in the $1^{st}$ order model. Given data collected under both nominal and disturbed conditions demonstrates that an irregularity detection algorithm is viable for monitoring the estimation process.

## TEC MEASUREMENTS

We set the stage for this analysis by stating the influence of the ionosphere on the GPS ranging signals. The frequency dependent delay (dispersion) observed by dual frequency reference stations is seen on both the carrier phase and pseudorange observations

$$\text{TEC}_\phi = \gamma\left(\phi_{L1} - \phi_{L2}\right) + N_{12} + IFB + \tau_{gd} \qquad (1)$$

and

$$\text{TEC}_\rho = \gamma\left(\rho_{L2} - \rho_{L1}\right) + M + \xi + IFB + \tau_{gd} \qquad (2)$$

where $\gamma = \frac{f_{L2}^2}{f_{L1}^2}$ converts the TEC into meters at $f_{L1}$, $N_{12}$ is the relative cycle ambiguity of the carrier phase measurement, $IFB$ is the receiver hardware bias, $\tau_{gd}$ is the satellite hardware bias, $M$ is multi-path, and $\xi$ is thermal noise in the receiver. Note that for the purposes of this work the noise and multi-path on the carrier phase measurement are considered to be negligible.

In order to achieve an improved ionospheric measurement the carrier and code measurements can be filtered together. This filtering process relies on the complementary nature of the two observations. The code is noisy but absolute whereas the carrier is very precise but biased by the cycle ambiguity. Consider the following truth measurement

$$\tilde{\text{TEC}} = \text{TEC}_\phi - \frac{1}{M}\sum_{m=0}^{t \text{ or } M}\left(\text{TEC}_\phi - \text{TEC}_\rho\right) \qquad (3)$$

where $M$ $(t)$ includes all (past) measurements in a continuous phase track and the biases, IFB and $\tau_{gd}$, have been calibrated out. Here the carrier ambiguity is resolved in real-time $(t)$ or post-processing $(M)$. The distinction is that the real-time filter is of course causal and cannot utilize measurements from the future. The post-processed truth can however average all the code measurements from a single carrier phase track against the carrier cycle ambiguity. Note that

in operation the filter implements a weighted average from the calibrated reference observations.

Figure 1 depicts an example of all three types of measurements, code, real-time carrier smoothed code, and the carrier phase reference from post-processing. In the process of collecting such measurements the receivers in the reference network are still prone to glitching and faults or residual measurement errors. In our analysis of the ionospheric correlation structure we require further processing to remove these faults.

The WAAS reference network contains triplicated receivers at each reference station. This redundancy can be used to effectively isolate and remove any remaining faults. At each epoch and for every reference station the three carrier reference measurements are compared to identify any outliers and if possible isolate them to resolve an accurate truth measurement. The resulting measurement, vTEC, has been dubbed a "supertruth" measurement and is achieved by the following expression

$$\text{vTEC} = \begin{cases} \frac{\Sigma_{i=1}^{3}\text{TEC}_i}{3\text{Ob}(H,el)} & \text{if } |\text{TEC}_i - \text{TEC}_j| < T \ \forall i,j = 1..3 \\ \frac{\Sigma_{i=1}^{2}\text{TEC}_i}{2\text{Ob}(H,el)} & \text{if } |\text{TEC}_i - \text{TEC}_j| < T \ \forall i,j = 1..2 \\ \text{NA} & \text{otherwise} \end{cases} \tag{4}$$

where $T = 30$cm is detection threshold for rejecting faulty measurements and

$$Ob(H, el) = \sec(\arcsin\left(\frac{R_e}{R_e + H}\cos el\right)) \tag{5}$$

is the so-called obliquity factor that converts the slant measurement into and equivalent vertical delay and the TEC observations are from Equation (3). A collection of 24 hours of supertruth measurements taken by the WAAS reference network (courtesy Raytheon Systems Corporation and JPL) are reported in Figure 2.

The supertruth measurements provide the fundamental quantities which are fed in to the correlation analysis process. Again this is all done in a post-processing mode so that we may extract measurements that are as clean as possible. Indeed we seek to identify the correlation structure of the ionosphere not the correlation structure of the reference receiver network. To that end we have collected data from the WAAS reference network under nominal conditions which exist the vast majority of the time and on those occasions where

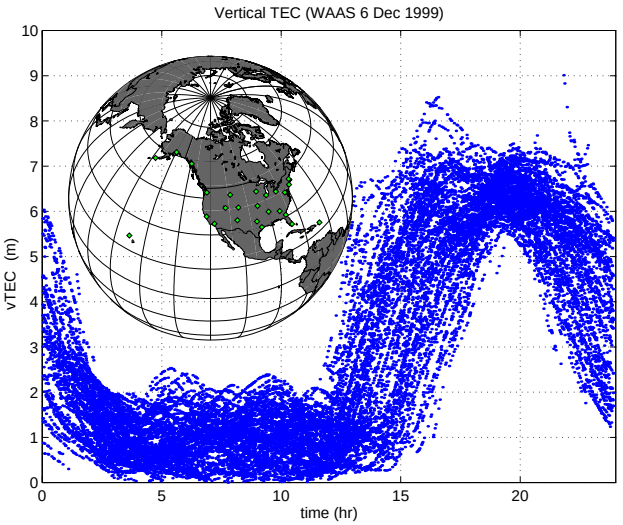

Figure 2: A 24hr collection of supertruth measurements take on 6 Dec 1999 show the diurnal variation of the vertical TEC. The CONUS reference network of triplicated receivers virtually removes all faulty ionospheric measurements.

the ionosphere transitions into a disturbed state to generate supertruth measurements for the analysis below.

In the following two sections we present data from 7 Jun 2000 and 2 Jul 2000 which represents nominal conditions. Note that data for 6 Dec 1999 has already been published [4]. Likewise data collected 6 April 2000 and 15-16 July 2000 is presented which represents disturbed conditions of the ionosphere where irregularities occur that directly influence the supertruth measurements and are reflected in the correlation metrics.

# $0^{th}$ ORDER CORRELATION

The primary goal of this section is to identify a correlation equation for the raw vertical ionospheric delay over CONUS. In order to identify this correlation structure we analyze differences between the vTEC supertruth measurements described in the previous section. As described in [4] the zeroth order decorrelation function is modeled as an additive quantity that prescribes the expected bound on the absolute difference between two vTEC measurements taken a given distance apart.

The decorrelation function took the form

$$\sigma_{\text{decorr}}(\text{GCD}) = m \times \text{GCD} + b \tag{6}$$

where $m$ was 50cm/Mm, GCD is the great circle distance between ionospheric pierce points, and $b$ is 50cm. The nominal data presented below reaffirms this model and the disturbed data clearly indicates where this model breaks down.

The correlation analysis is presented graphically here in a series of four panels, each panel containing three graphs which lead from raw vTEC differences to the affine model of Equation (6). We used the first panel (Figure 3) as an example for description. The top graph is a two dimensional histogram that plots bins of vertical ionospheric differences versus great circle distance separating ionospheric pierce points. For each pair of measurements in one epoch of the time history like Figure 2 but taken 7 Jun 2000, the bin corresponding to the ordered pair ($\Delta$vTED, GCD$_{ij}$) is incremented where $\Delta\text{vTED} = |\text{vTEC}_i - \text{vTEC}_j|$. The histogram is then plotted on a logarithmic scale to achieve the surface shown.

The middle graph in Figure 3 contains a family of 40 curves, one for each GCD bin. Here, the horizontal axis indicates $\Delta$vTEC for each curve and the vertical curve indicates the likelihood of occurrence. In order to read this chart, first choose the curve corresponding to the GCD separation bin you wish to examine, then select the vertical TEC difference on the horizontal axis that you would like to bound. The intersection of that $\Delta$vTEC value and the chosen curve tells you the probability that a pair of measurements separated by that GCD.

The bottom graph in Figure 3 identifies the additive correlation model for the raw ionosphere. It contains four curves corresponding to the 68%, 95%, 99%, and 99.9% values for bounding the probability curves in the middle graphic. It is plotted on the same two dimensional axis as the decorrelation histogram in the top graphic, $\Delta$vTEC versus GCD and is constructed by integrating out the 68%, 95%, 99%, and 99.9% values in each GCD bin of the decorrelation histogram and projecting them down to the equivalent standard deviation of a normal distribution. For example, at GCD = 2000km, in the top graph of Figure 3, 99.9% of the counts fall below 6m and 6m/3.29 $\approx$ 1.8m, so that the 99.9% curve intercepts 2000km at 1.8m. Note that the multipliers for these four percentages are 68%–1, 95%–2, 99%–2.58, 99.9%–3.29. To achieve meaningful projections at higher percentiles would require a larger data sample.

The dramatic result of the ionospheric correlation analysis for the vast majority of time is the regularity of the ionospheric distribution over CONUS. The family of cumulative likelihood curves exemplifies this in both the shortness of tails (curves bending downward) and the monotonic increase in difference versus distance where the left-most line corresponds to 100km with curves increasing to the right-most at 2000km. If the individual curves in the probability chart (middle graph) cross in a significant manner, this indicates that small scale irregularities exist without the presence (or at least observation of) larger scale irregularities.

A second example of correlation analysis on a nominal ionospheric day, 2 Jul 2000, is given in Figure 4. There the graphics in the full panel are essentially indistinguishable from the 7 Jun 2000 data and likewise if compared against the 6 Dec 1999 day support the decorrelation model expressed above.

We now turn to the data sets where other ionospheric indicators such as the Kp and Ap indices and EUV images suggest ionospheric activity that is out of the ordinary. Here two sets of data were taken at times when these traditional indices would suggest ionospheric storm conditions, although not necessarily severe in nature. They are 6 Apr 2000 and 15-16 Jul 2000. These results clearly show deviation from the nominal model. In an overall sense this is identified in the bottom chart showing the bounding standard deviations where the various percentiles do not project to the same standard deviation. This indicates an increase in the tails of the distribution. Likewise this shows up in the probability plots as a flattening of the curves, that is they do not roll off as quickly.

An important observation here however is that the monotonicity of the probability curves is preserved. This is reassuring in that the irregularities seen at shorter GCD separations are accompanied by irregularities at larger separations. The implication is that the estimation and integrity algorithms irregularities are well well equipped with reference measurements to observe the irregularities and protect the users by increasing the confidence bounds on the ionospheric correction.

## $1^{st}$ ORDER CORRELATION

In this section we present a decorrelation model very similar to that presented above with the exception that a planar fit of vertical ionosphere has been removed from the raw measurements. The purpose

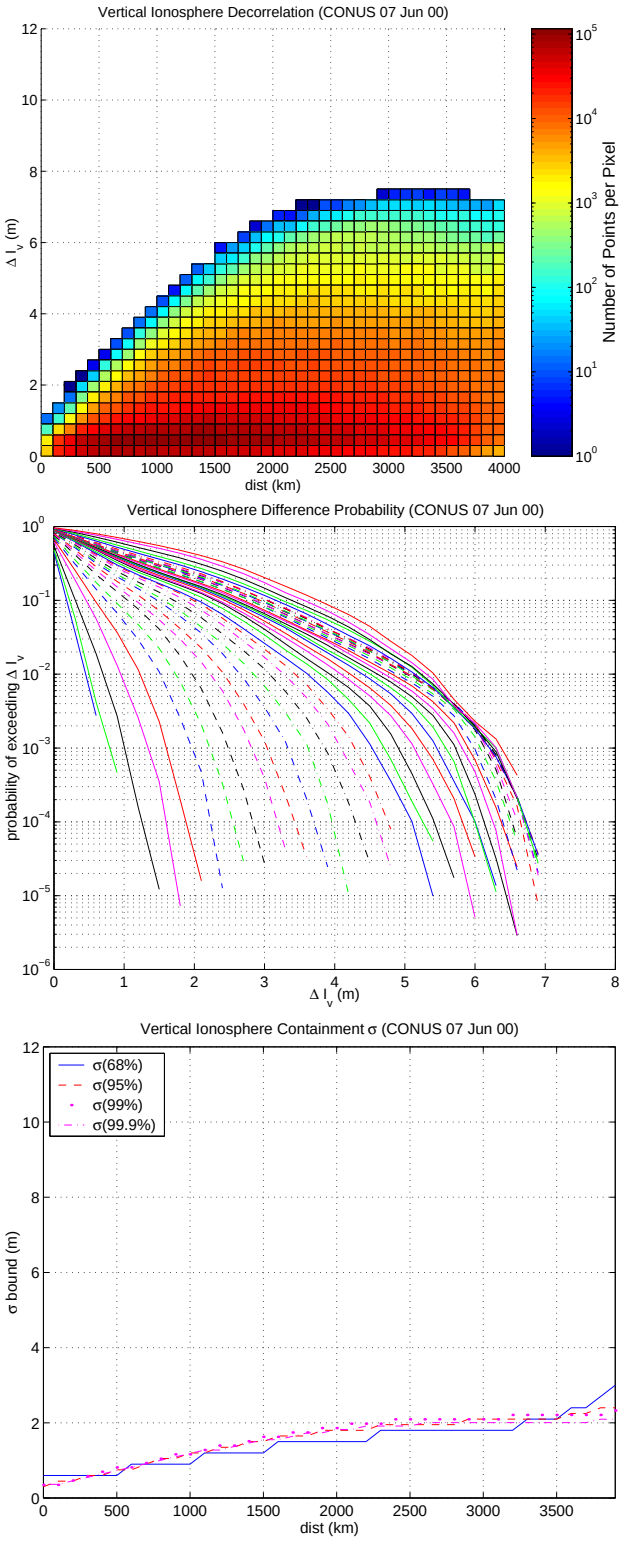


Figure 3: The two dimensional histogram of vertical ionospheric differences v. pierce point great circle separation shows the clean correlation structure of the ionosphere expected in CONUS is given in the top graphic. The family of cumulative likelihood curves showing occurrence rate of a given vTEC difference at a given GCD is plotted in the middle graphic. The family of bounding standard deviations predicted by the selected percentiles presuming a normal distribution are shown in the bottom graphic.

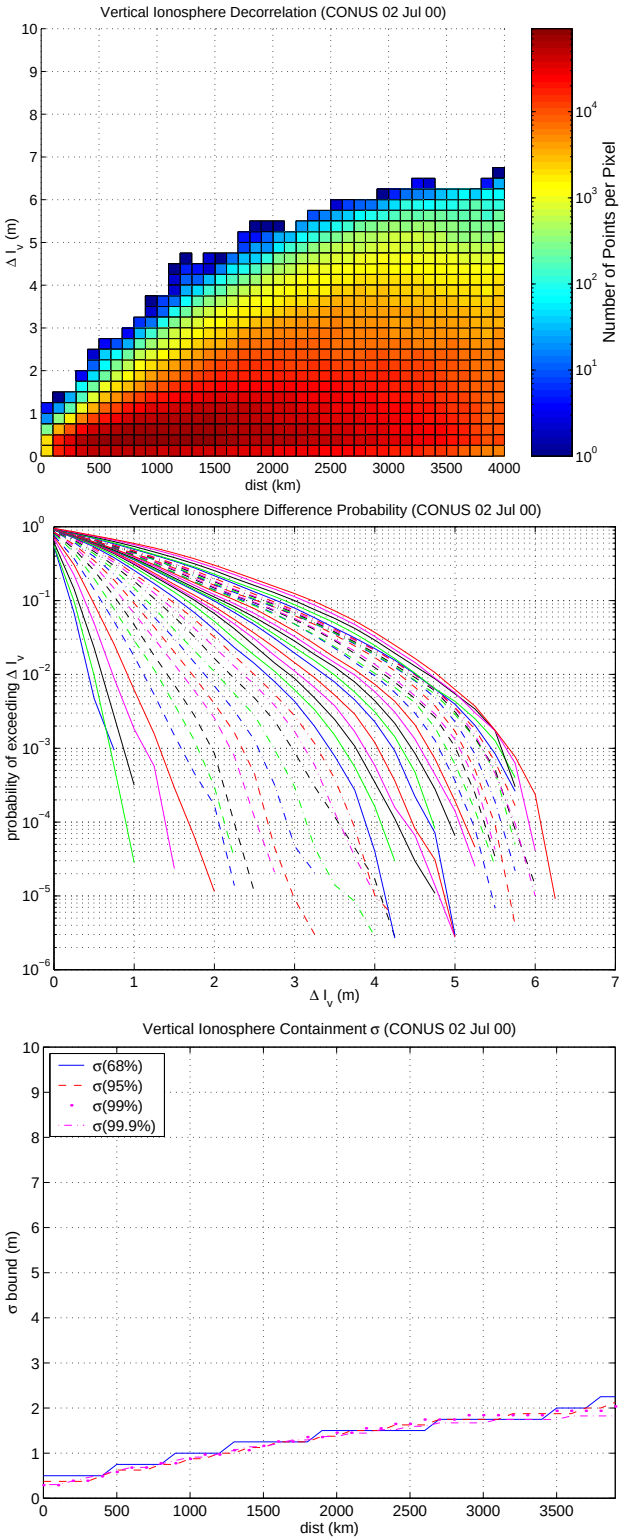


Figure 4: Above is data taken 2 Jul 2000 and processed in identically the same fashion as that in Figure 3. Again the well behaved ionosphere has clean and truncated tails that defines a quiet ionosphere for WAAS.

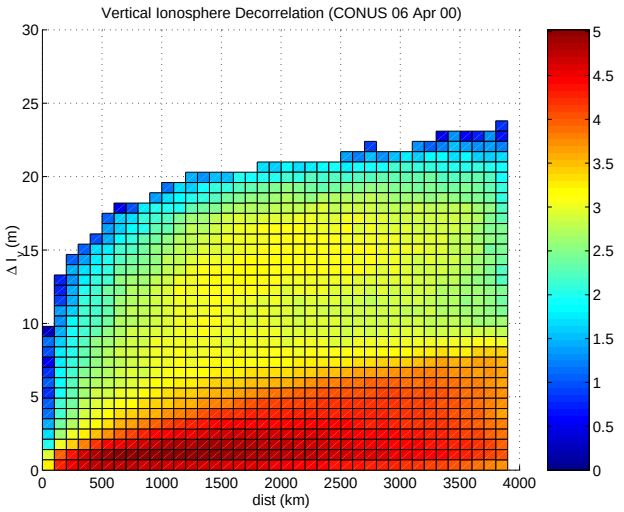


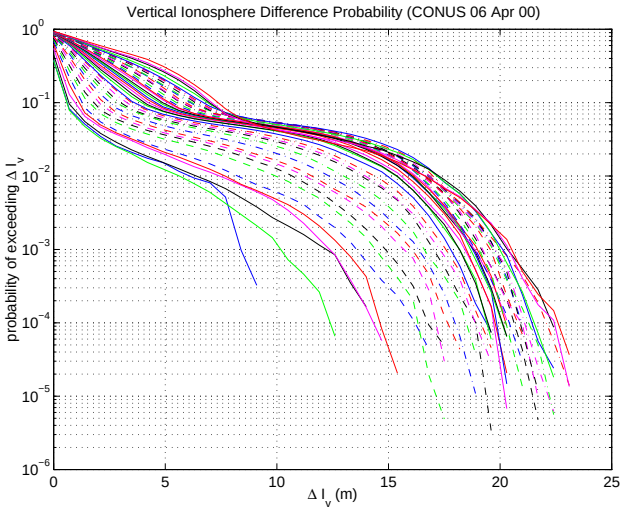


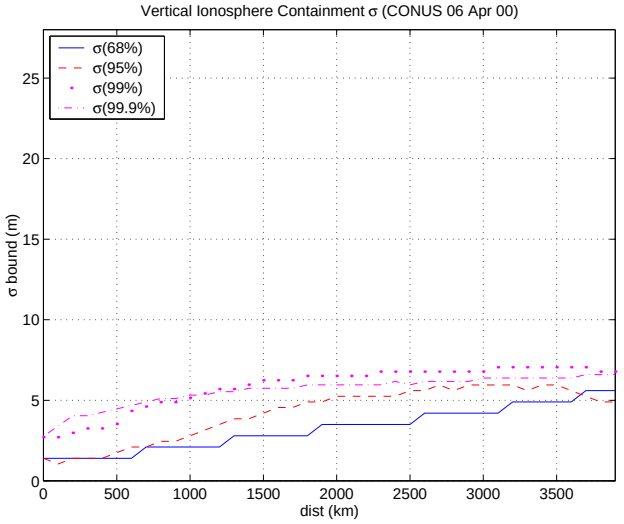


Figure 5: The data in this figure was collected 6 Apr 2000 and represents an ionospheric distribution that is not well behaved and contains observations of ionospheric irregularities that violate the correlation structure seen in the quiet or nominal ionospheric distribution. Notice the tail behavior in the cumulative probabilities where the shelf at around 10m pushes to the right before eventually tailing off. The standard deviation of measurement differences does not follow a normal model.

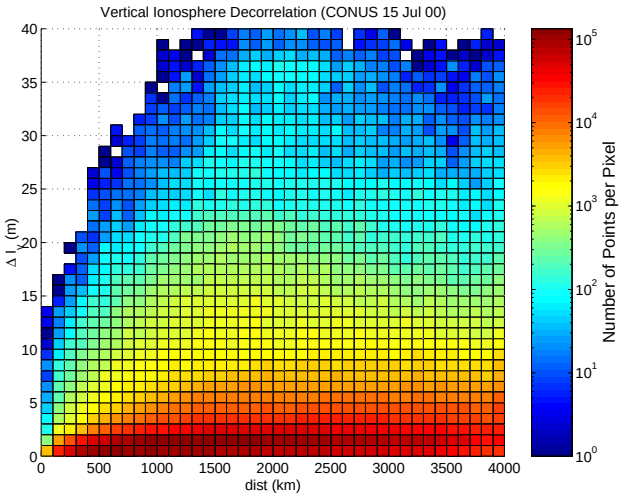


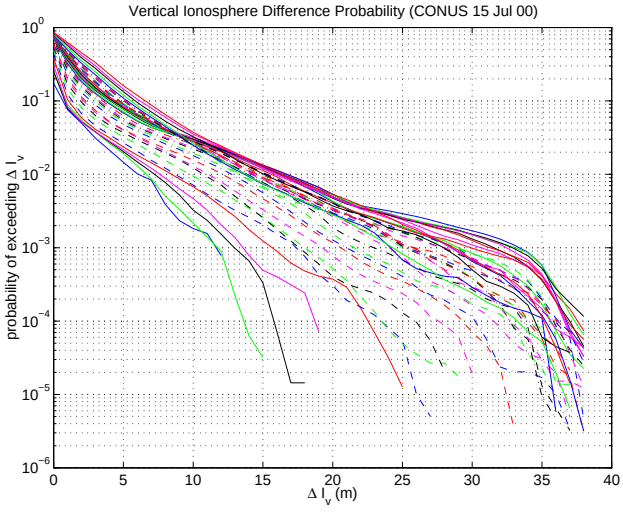


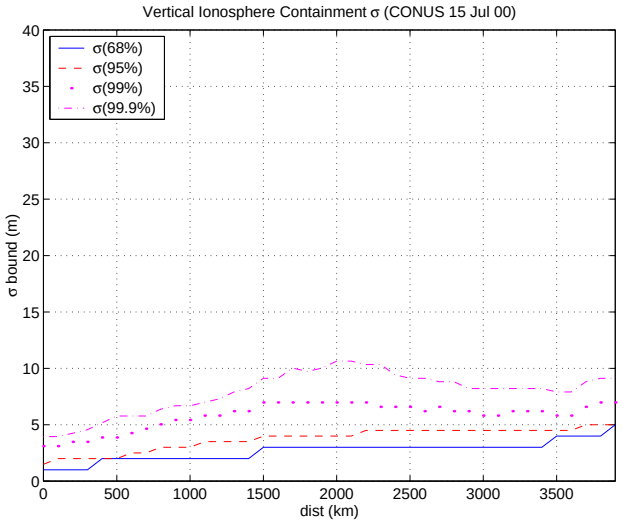


Figure 6: Above is another collection of irregular ionospheric observations taken 15-16 Jul 2000. This captures the most extreme gradients yet observed with the WAAS reference network over CONUS. Some time over the course of this day, vertical ionospheric measurements separated by 100km or less were different by more than 13 meters. Here the irregularities in the ionosphere cover a much broader geographic scale changing the overall slope rather than introducing a shelf.

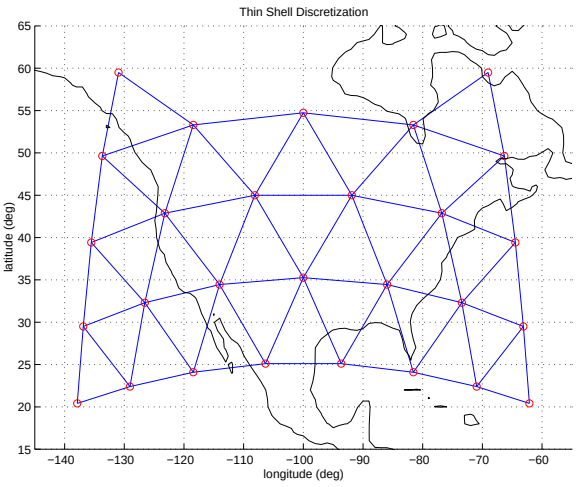


Figure 7: The thin shell ionosphere is discretized into equal area triangles whose vertices serve as origins for locally planar coordinate systems used to estimate the vertical ionosphere.

for doing this is to loosely mimic the WAAS ionospheric correction process over the collection of supertruth measurements and generate a complete set of first order residuals. These residuals provide the fundamental quantities fed to the first order correlation analysis process. The motivation for a first order decorrelation model is an accurate covariance propagation in the WAAS ionospheric irregularity detector [5] which performs a $\chi^2$ check to test the estimator's goodness-of-fit..

Beginning with the same supertruth measurements as above and the locations of the pierce points a locally planar estimate is generated at each vertex of a geodesic sphere located at 350km altitude over CONUS as in Figure 7. The linear estimate of planar vertical ionosphere at each vertex is then

$$\widehat{\mathrm{vTEC}} = \mathbf{A}^{+}\mathrm{vTEC} \tag{7}$$

where $\mathbf{A} \in \mathbb{R}^{m\times 3}$ is the observation matrix

$$\mathbf{A} = \begin{bmatrix} 1 & \delta\hat{E}_1 & \delta\hat{N}_1 \\ 1 & \delta\hat{E}_2 & \delta\hat{N}_2 \\ \vdots & \vdots & \vdots \\ 1 & \delta\hat{E}_m & \delta\hat{N}_m \end{bmatrix} \tag{8}$$

for the $m$ measurements within a disc of radius GCD $< R$ of the given vertex. The residual ionosphere is

$$\delta\mathrm{vTEC}_1 = \widehat{\mathrm{vTEC}}(r_1) - \mathrm{vTEC}_1 \tag{9}$$

and

$$\nabla\Delta\mathrm{vTEC} = |\delta\mathrm{vTEC}_1 - \delta\mathrm{vTEC}_2| \tag{10}$$

is then the analyzed quantity instead of $\Delta$vTEC as in the previous section. We see from the analysis of nominal data in Figures 8 and 9 that a reasonable model of the residual decorrelation function is a constant

$$\sigma_{\mathrm{decorr}}(\mathrm{GCD}) = b \tag{11}$$

where $b$ is somewhere between 35cm and 50cm. In contrast the data from the disturbed ionospheric conditions contain irregularities that are distinct from the nominal profile. The residual differences therefore provide a test quantity for the irregularity detector to monitor. Further the monotonicity of the residual probability charts again supports the assumption that small scale irregularities are accompanied by larger scale irregularities.

## ACKNOWLEDGMENTS

The authors wish to thank Drs. Byron Iijima and Tony Mannucci of the Jet Propulsion Laboratory and Eric Altshuler and Mine Hagen of Raytheon Systems Corporation for supplying raw data and post-processed measurement data from the WAAS reference network. Likewise we appreciate the questions and subsequent guidance from the WAAS Ionospheric Performance Panel that spurred this work We gratefully acknowledge the FAA Satellite Navigation Program Office for sponsoring GPS engineering and research in aviation at Stanford.

## REFERENCES

[1] C. Kee, B. W. Parkinson, and P. Axelrad, "Wide area differential GPS," *Navigation*, vol. 38, Summer 1991.

[2] P. Enge, T. Walter, S. Pullen, C. Kee, Y.-C. Chao, and Y.-J. Tsai, "Wide area augmentation of the the Global Positioning System," *Proceedings of the IEEE*, vol. 84, no. 8, pp. 1063–1088, 1996.

[3] T. Walter, A. J. Hansen, and P. Enge, "Validation of the WAAS MOPS integrity equation," *Proceedings of the Institute of Navigation Annual Meeting*, pp. 217–26, June 1999.

[4] A. J. Hansen, E. Peterson, T. Walter, and P. Enge, "Correlation structure of ionospheric estimation and correction for waas," *Proceedings of the Institute of Navigation National Technical Meeting*, pp. 454–63–9, January 2000.

[5] Todd Walter, et.al., "Robust detection of ionospheric irregularities," *Proceedings of the Institute of Navigation GPS-93*, September 2000.

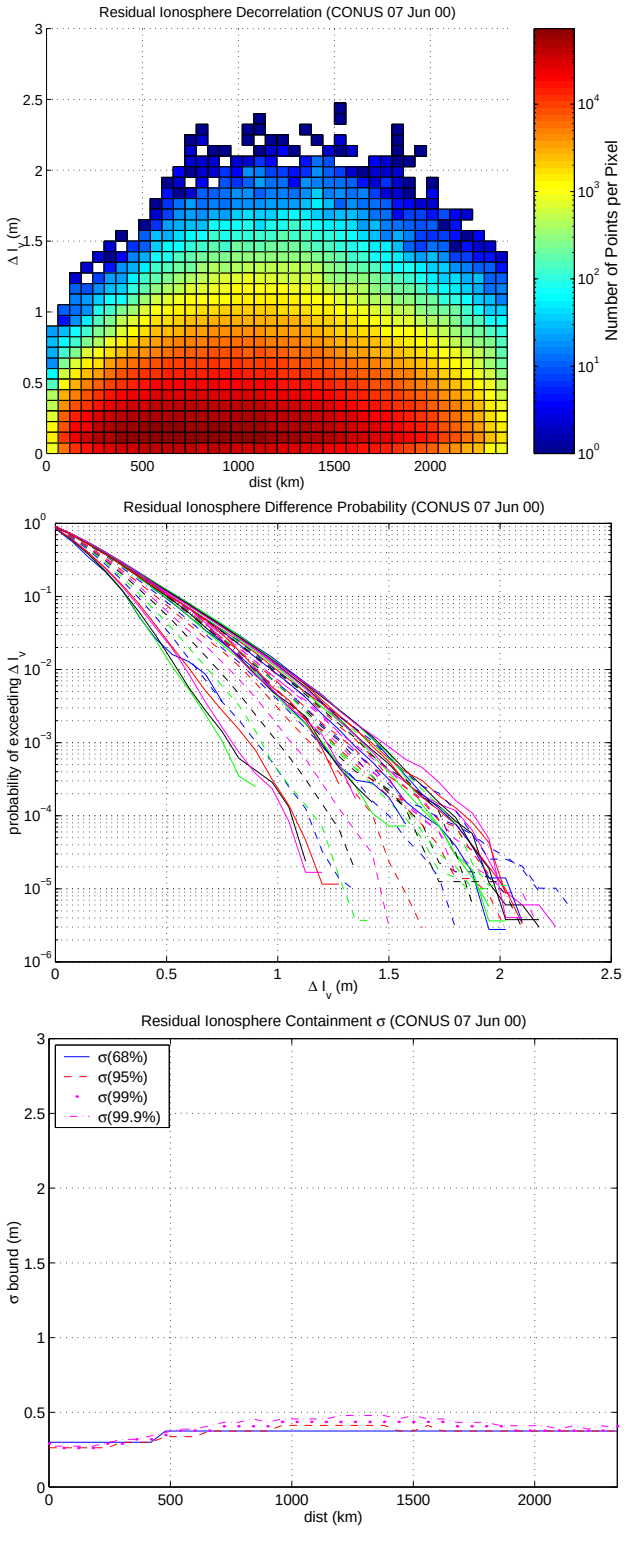


Figure 8: The two dimensional histogram here has exactly the same form as the zeroth order plots with the exception that the vertical axis now reports the difference of two residuals rather than the difference of two raw measurements. Likewise the difference axis in the middle and bottom graphs also depict residual ionospheric differences rather than raw measurement differences.

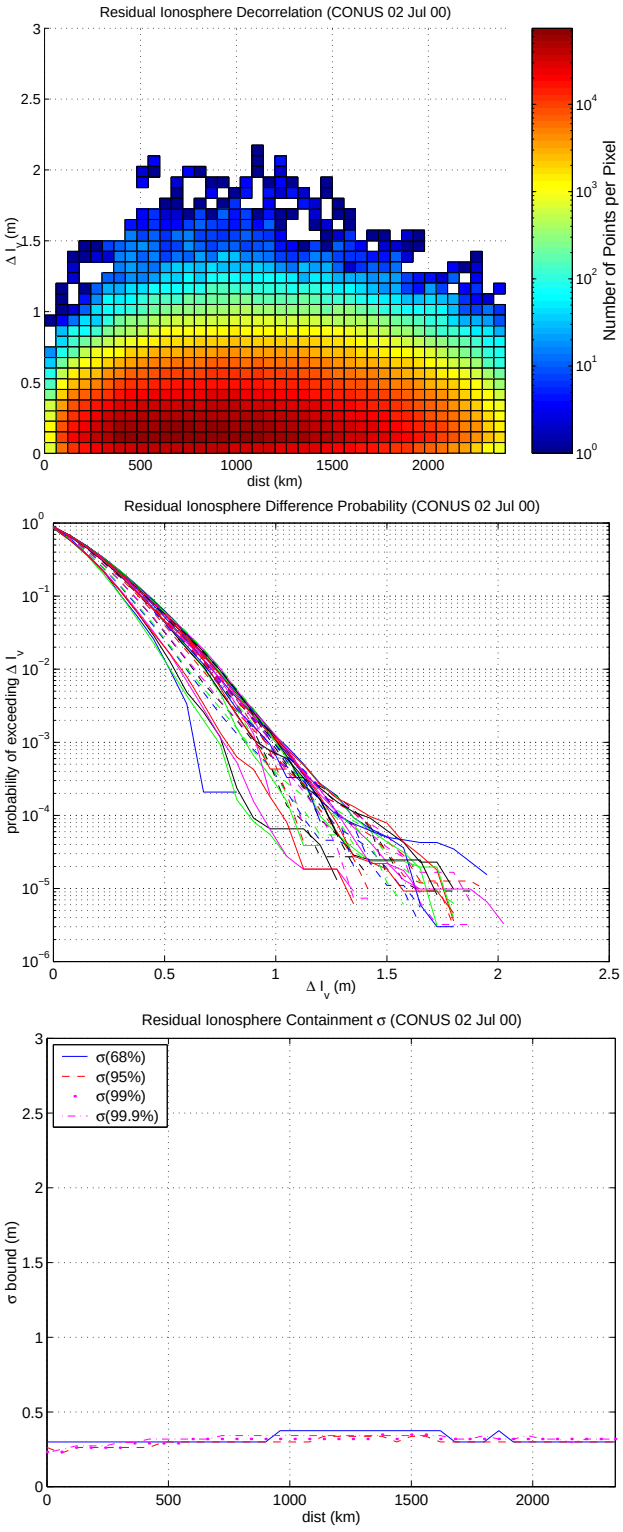


Figure 9: Above is data taken 2 Jul 2000 and processed in identically the same fashion as that in Figure 8. Again the well behaved ionosphere has clean and truncated tails that defines a quiet ionosphere for WAAS.

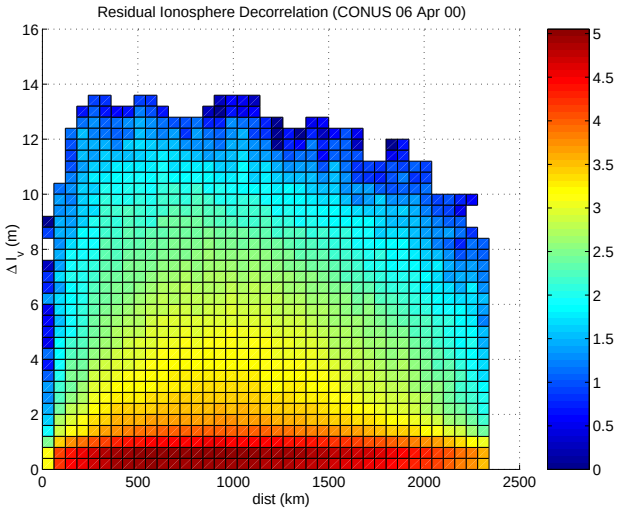


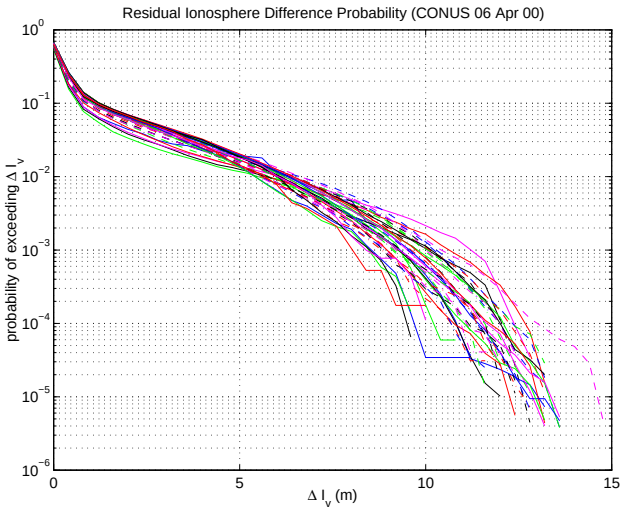


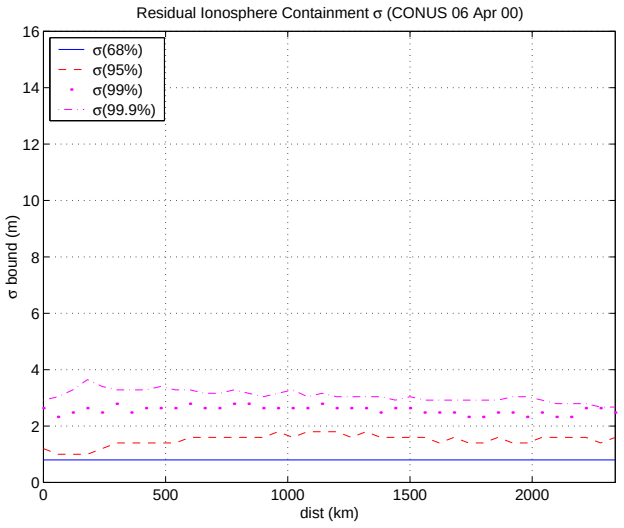


Figure 10: The data in this figure was collected 6 Apr 2000 and represents an residual distribution that is not well behaved and contains irregularities that are not well model as a plane.

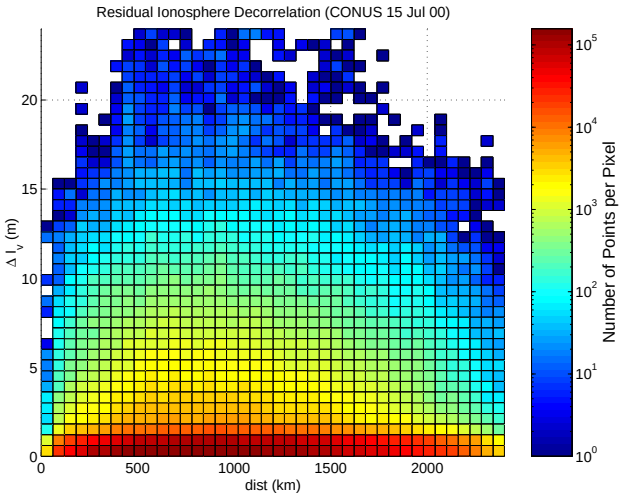


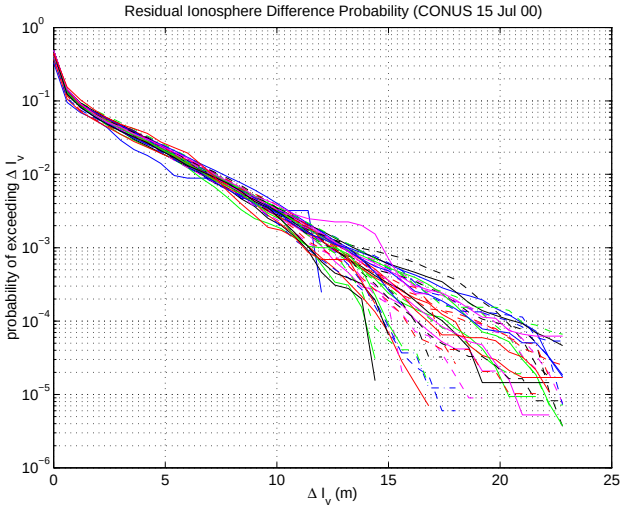


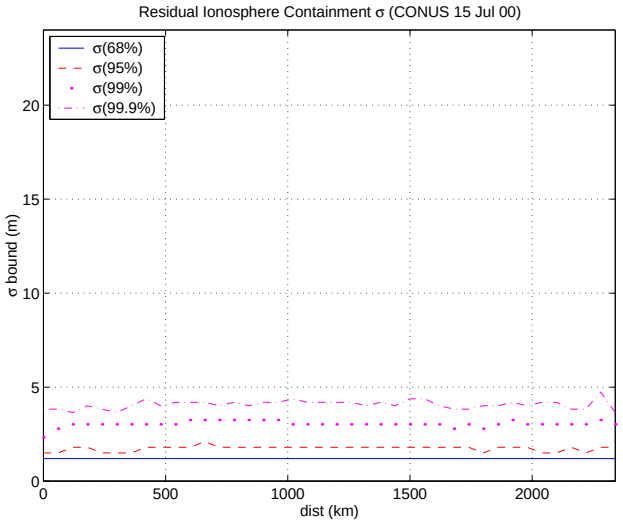


Figure 11: Above is the final collection of irregular ionospheric residuals taken 15-16 Jul 2000. The slope of the entire probability curve (middle graph) is flattened indicating that the residuals are uniformly larger over CONUS. While this impacts availability by requiring increased confidence bounds it does not compromise the integrity of the ionospheric corrections as the integrity algorithm is sensitive to this through its underlying measurements.